

Electronic Supplementary Information

NO-responsive Probe for Detecting Acute Inflammation with NIR-II Fluorescence/Optoacoustic Imaging

Zunpan She, Junjie Chen, Lihe Sun, Fang Zeng* and Shuizhu Wu*

State Key Laboratory of Luminescent Materials and Devices, Guangdong Provincial Key
Laboratory of Luminescence from Molecular Aggregates, College of Materials Science and
Engineering, South China University of Technology, Guangzhou 510640, China

[*] Corresponding authors

E-mail: mcfzeng@scut.edu.cn

shzhwu@scut.edu.cn

Table of contents

General experimental procedures	S3
Scheme S1	S8
Fig. S1	S9
Fig. S2.....	S9
Fig. S3.....	S10
Fig. S4.....	S11
Fig. S5.....	S11
Fig. S6.....	S12
Fig. S7.....	S12
Fig. S8.....	S13
Fig. S9.....	S14
Fig. S10.....	S15
Fig. S11.....	S16
Fig. S12.....	S16
Fig. S13.....	S17
Fig. S14.....	S17
Fig. S15.....	S18
Fig. S16.....	S19
Fig. S17.....	S19
Fig. S18.....	S20
Fig. S19.....	S21
Fig. S20.....	S21
Fig. S21.....	S22
Fig. S22.....	S23
Fig. S23.....	S23
Fig. S24.....	S24
Table. S1	S25
References	S27

General experimental procedures

1. Reagents.

Cyclopentanone, phosphorus oxychloride, 1,1,2-trimethylbenz[e]indole, methylamine hydrochloride and triethylamine were purchased from Energy Chemical Reagents. DMEM and 10% phosphate buffer saline (PBS) were purchased from KeyGen Bio-Tech. MAHMA NONOate (NO donor, chemical name: (Z)-1-[N-Methyl-N-[6-(N-methylammoniohexyl)amino]]diazene-1,2-diolate, also known as methylamine hexamethylene methylamine NONOate) was purchased from Sigma-Aldrich (St. Louis, MO, USA). The solvents including tetrahydrofuran (THF), N, N-Dimethylformamide (DMF) and dichloromethane (DCM) of analytical grade were dried with molecular sieve and distilled before use. Other solvents used in this study were analytical grade reagents and used without further purification. The water used in the experiments was the triple-distilled water. The PBS is pH 7.4 at the concentration of 10 mM.

2. Apparatus.

Nuclear magnetic resonance (NMR) spectra were measured on AVANCE III HD 500 NMR spectrometer. High resolution mass spectrometer (MS) was recorded on a Bruker MAXIS IMPACT mass spectrometer. The Near-Infrared II (NIR-II) fluorescence spectra were obtained on NIRQUEST512 spectrometer (excitation: 808 nm laser, emission range: 900-1700 nm). The absorption spectra were collected on Hitachi U-3010 spectrophotometer. The NIR-II fluorescence (in vivo and ex vivo) imaging was performed by using NIR-II in Vivo Fluorescent Imaging System (Series II 808/900-1700, Suzhou NIR-Optics Technologies Co., Ltd.). Optoacoustic imaging was performed by inVision128 multispectral optoacoustic tomographic (MSOT) imaging system (iThera Medical GmbH).

3. Syntheses.

Synthesis of compound 1. Compound 1 was prepared as described previously ^[1].

Synthesis of compound 2. Compound 2 was prepared as described previously ^[2].

Synthesis of compound 3. Under nitrogen atmosphere, Compound 1 (712 mg, 2 mmol) and Compound 2 (158 mg, 1 mmol) were added to a 100 ml two-neck round-bottom flask.

Then acetic anhydride (10 mL) was added to dissolve them. Subsequently, sodium acetate (164 mg, 2 mmol) was added to the flask. The reaction mixture was stirred and heated to 80 °C for 2 h. After cooling to room temperature, the solvent was removed by evaporation under reduced pressure, and the residue was subjected to silica gel chromatography with CH₂Cl₂/CH₃OH (20/1, v/v) as eluent to afford a deep green solid. Yield: 538 mg (65%). ¹H NMR (500 MHz, CDCl₃) δ 8.03 (d, J = 8.5 Hz, 2H), 7.85 (t, J = 8.6 Hz, 6H), 7.50-7.54 (m, 4H), 7.39 (t, J = 7.5 Hz, 2H), 6.23 (d, J = 14.1 Hz, 2H), 4.55 (s, 4H), 3.94 (t, J = 4.7 Hz, 4H), 3.55 - 3.57 (m, 4H), 3.46 - 3.48 (m, 4H), 3.40 (t, J = 4.6 Hz, 4H), 3.28 - 3.30 (m, 4H), 3.20 (s, 6H), 2.99 (s, 4H), 1.94 (s, 12H). HR-MS (ESI, m/z) calcd for [C₅₁H₆₃ClN₂O₆]⁺ [M+H]⁺ 833.4375, found 833.4319.

Synthesis of compound HC-N. A mixture of Compound 3 (167 mg, 0.2 mmol) and methylamine hydrochloride (135 mg, 2 mmol) was dissolved in anhydrous DMF (5 mL) under nitrogen atmosphere. Subsequently, triethylamine (70 μL, 0.5 mmol) was added to the solution. The mixture was stirred and heated to 65 °C for 1 h. After cooling to room temperature, the mixture was dissolved in CH₂Cl₂ (50 mL), followed by washing with water three times and drying by Na₂SO₄. The solvent was removed by evaporation under reduced pressure, and the residue was subjected to silica gel chromatography with CH₂Cl₂/CH₃OH (30/1, v/v) as eluent to afford a deep red solid. Yield: 103 mg (62%). ¹H NMR (500 MHz, DMSO-d₆): δ 8.07-8.14 (m, 4H), 7.93 - 7.98 (m, 4H), 7.54 - 7.59 (m, 4H), 7.39 (t, J = 7.5 Hz, 2H), 5.74 (d, J = 12.6 Hz, 2H), 4.26 (s, 4H), 3.80 (s, 4H), 3.53 (d, J = 5.2 Hz, 4H), 3.42 - 3.44 (m, 4H), 3.36 - 3.38 (m, 4H), 3.24 - 3.26 (m, 4H), 3.13 (s, 6H), 2.77 (s, 4H), 2.51 (s, 3H), 2.29 (s, 1H), 1.93 (s, 12H). ¹³C NMR (126 MHz, DMSO-d₆): δ 165.38, 146.24, 141.52, 138.06, 130.81, 130.64, 130.28, 130.03, 128.52, 128.30, 127.72, 125.99, 123.90, 122.12, 111.76, 96.73, 71.63, 70.81, 70.27, 70.08, 67.79, 58.42, 49.31, 43.48, 34.37, 27.40, 26.28, 21.26. HR-MS (ESI, m/z) calcd for C₅₂H₆₆N₃O₆ [M]⁺ 828.4946, found 828.4972.

4. Optical response of the probe toward NO.

MAHMA NONOate was used as the NO donor. HC-N test solutions was prepared, after the addition of NO donor (0-50 μM), the test solutions (with HC-N final concentration of 5.0 μM.) were allowed to incubate for 10 min at 37 °C, and their absorption and fluorescent

spectra were recorded. In time-dependent experiments, the spectra of the test solutions were obtained at different time periods after the probe's incubation with NO. In selectivity-evaluation experiments, the spectra of test solutions were obtained at 10 min after adding NO donor or other substances. Probe stock solution was prepared in EtOH. The excitation light in NIR-II fluorescent spectra measurement was an 808 nm laser at a power density of 70 mW cm⁻² and the OA intensities were recorded at 865 nm.

5. Cell experiments.

Mouse fibroblast cells (L929 cells) were obtained from Jiangsu KeyGEN BioTECH Co., Ltd. and cultured in Dulbecco's modified Eagle's medium (DMEM) containing 10% fetal bovine serum (FBS) and 1% penicillin and streptomycin at 37 °C with 5% CO₂ humidified atmosphere.

Methyl thiazolyl tetrazolium (MTT) assay was conducted to investigate the in vitro cytotoxicity of the probe HC-N. In short, L929 cells were seeded into 96-well plates at a cell density of 5000 cells/well and were allowed to grow for 24 h. Then, the medium in each well was discarded, and the cells were washed with PBS three times which were followed by another 24 h culture with fresh medium containing different concentrations (0, 10, 20, 30, 40 and 50 μM) of the probe HC-N. Next, each well was washed with PBS, and the cells were allowed to grow in the medium containing 0.5 mg mL⁻¹ MTT for 2 h. Then, the culture medium containing MTT was discarded, and DMSO (150 μL) was added into each well to dissolve the precipitates. Finally, the absorbance at 570 nm for each well was provided by Thermo MK3 ELISA reader to reflect the cell viability. In this experiment, 3 independent experiments were repeated and 8 replicates were measured for each concentration of the nanoprobe in every 96-well plates. Finally, the statistical mean and standard deviation were employed to estimate cell viabilities.

6. Phantom optoacoustic imaging.

The test solutions containing 5 μM HC-N in PBS (10 mM, pH = 7.4) and varied concentrations of MAHMA NONOate (0, 5, 10, 20, 30, 40, 50 μM) were stirred for 10 min at 37 °C. Then the solutions were added into commercial Wilmad NMR tubes for phantom

optoacoustic imaging which was conducted with MSOT system. The OA images were reconstructed at 865 nm with the back-projection reconstruction method.

7. Animal experiments.

Specific-pathogen-free (SPF) male BALB/c mice (6-7 weeks old) were provided by Guangdong Medical Laboratory Animal Center and kindly kept in the Laboratory Animal Center of South China Agricultural University. All mice had ad libitum access to SPF diet and sterile water and kept under a 12 h light/dark cycle. Mice housing and all in vivo experiments were approved by the Ethics Committee of Laboratory Animal Center from South China Agricultural University and performed following the institution's regulations as well as in accordance with the Regulations on the Management of Laboratory Animals of China. Before imaging experiments, depilation was conducted for the mice using a commercial depilatory agent. In imaging experiments, mice were randomly divided into 3 mice in each group.

8. Mouse model of lipopolysaccharides (LPS)-induced acute dermatitis

For the lipopolysaccharides (LPS)-induced acute dermatitis, mice were subcutaneously injected with LPS (9 mg kg⁻¹, in 50 μL saline) in right back skin region. Meanwhile, the mice were subcutaneously injected with the same volume of saline in the left back skin as the control. At 6 h, 12 h or 24 h after LPS treatment on the right back skin region and saline treatment on the left back skin region, the mice were subcutaneously injected with the probe (3.5 mg kg⁻¹, in 50 μL saline), and there were three mice per group.

9. Mouse model of monosodium iodoacetate (MIA)-induced acute joint inflammation

For the monosodium iodoacetate (MIA)-induced acute joint inflammation, mice were infrapatellar injected with MIA (13.5 mg kg⁻¹, in 20 μL saline) in right knee joint. Meanwhile, the mice were infrapatellar injected with the same volume of saline in the left knee joint as the control. At 12 h, 24 h or 48 h after MIA treatment in the right knee joint and saline treatment in the left knee joint, the probe (3.5 mg kg⁻¹, in 20 μL saline) was injected in situ into the mice, and there were three mice per group.

10. NIR-II Fluorescence imaging

In the experiments, after different groups of mice were anesthetized with 2% isoflurane in oxygen and HC-N (3.5 mg kg^{-1}) was injected in situ for NIR-II fluorescence imaging in vivo. The NIR-II fluorescence images were taken with NIR-II in Vivo Imaging System (excitation: 808 nm laser with $50 \text{ mW}\cdot\text{cm}^2$, emission filter: 900-1700 nm).

11. Optoacoustic imaging

For in vivo optoacoustic experiment, mice were given an injection of probe HC-N ($3.5 \text{ mg}\cdot\text{kg}^{-1}$) via in situ injection. Then the mice were anesthetized with continuous isoflurane with oxygen flow and placed in the animal holder for imaging at several time periods post in situ probe injection. The following wavelengths were selected based on the major turning points in the absorption spectra of HC-N, Hb and HbO₂: 700 nm, 715 nm, 730 nm, 750 nm, 800 nm, 830 nm, 865 nm, 880 nm and 900 nm (background). 10 individual frames at each wavelength were recorded. Cross-sectional images were acquired with a step size of 0.5 mm spanning through the whole scanning region.

12. H&E staining analysis

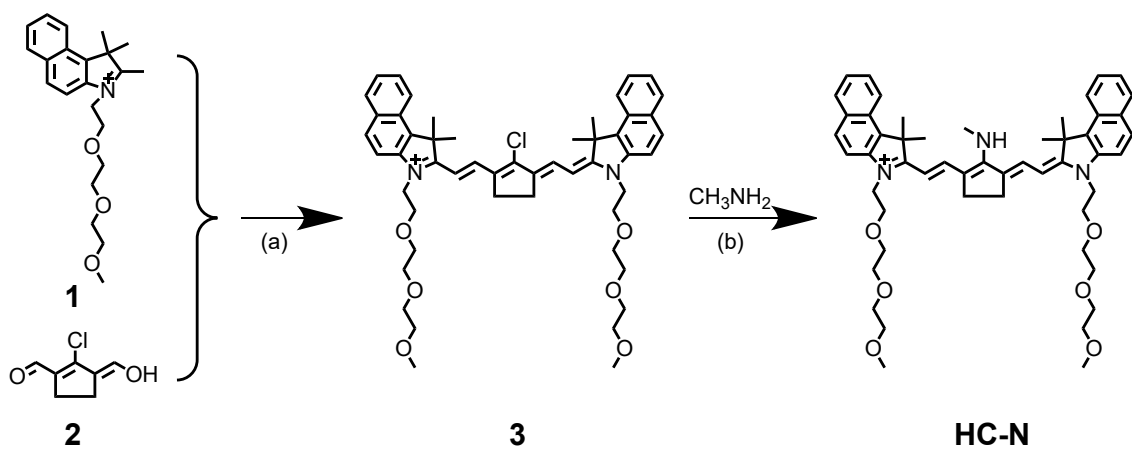
Organs were dissected and immersed in 10% formalin for 24 h. All the fixed organs were processed for paraffin embedding, sectioned, and stained with hematoxylin and eosin (H&E). For biosafety assessment, healthy mice were i.v. injected with an equal volume of saline or the probe, and the major organs (including heart, liver, spleen, lung and kidney) were dissected and subjected to H&E staining at 7 d after saline or probe injection.

13. Relative Optoacoustic (OA) intensity

Relative OA intensity was calculated with the equation:

$$\text{Relative OA intensity} = [(OA_{865})_{\text{NO}} - (OA_{865})_{\text{control}}] / (OA_{865})_{\text{control}}$$

where $(OA_{865})_{\text{NO}}$ is the OA intensity at 865 nm of HC-N in PBS treated with MAHMA NONOate, $(OA_{865})_{\text{control}}$ is the OA intensity at 865 nm of the control (PBS).



Scheme S1. Synthetic route for HC-N.

Reagents and conditions: a) Acetic anhydride, sodium acetate, 80 °C, N_2 , 2 h; b) DMF, methylamine hydrochloride, triethylamine, 65 °C, N_2 , 1 h.

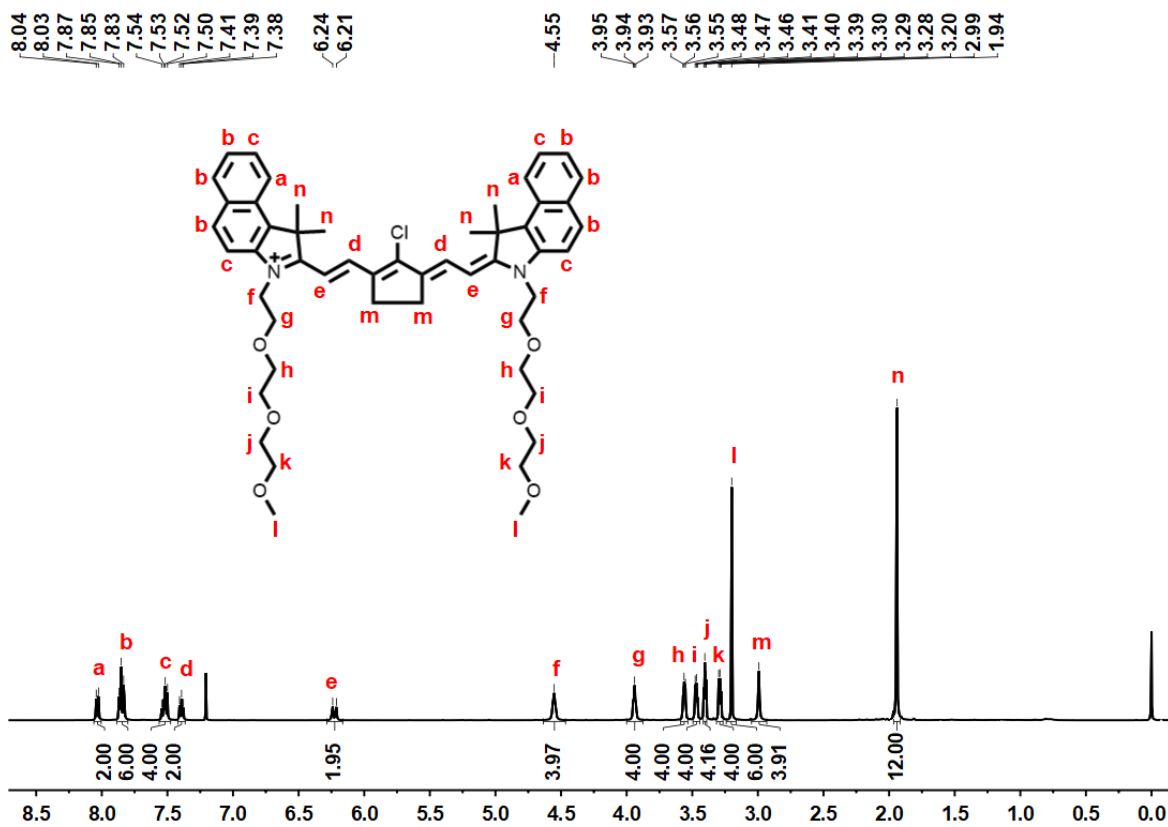


Fig. S1. ^1H NMR spectrum of Compound 3 in CDCl_3 .

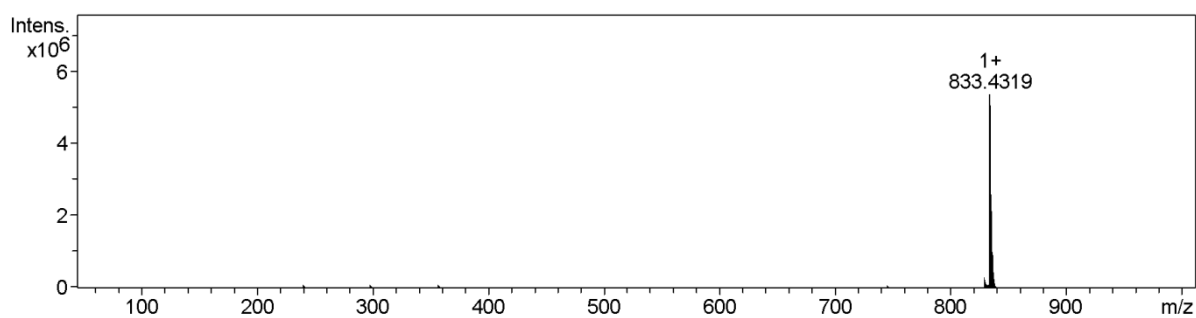


Fig. S2. HR Mass spectrum of Compound 3.

m/z $[\text{M}+\text{H}]^+$ 833.4319

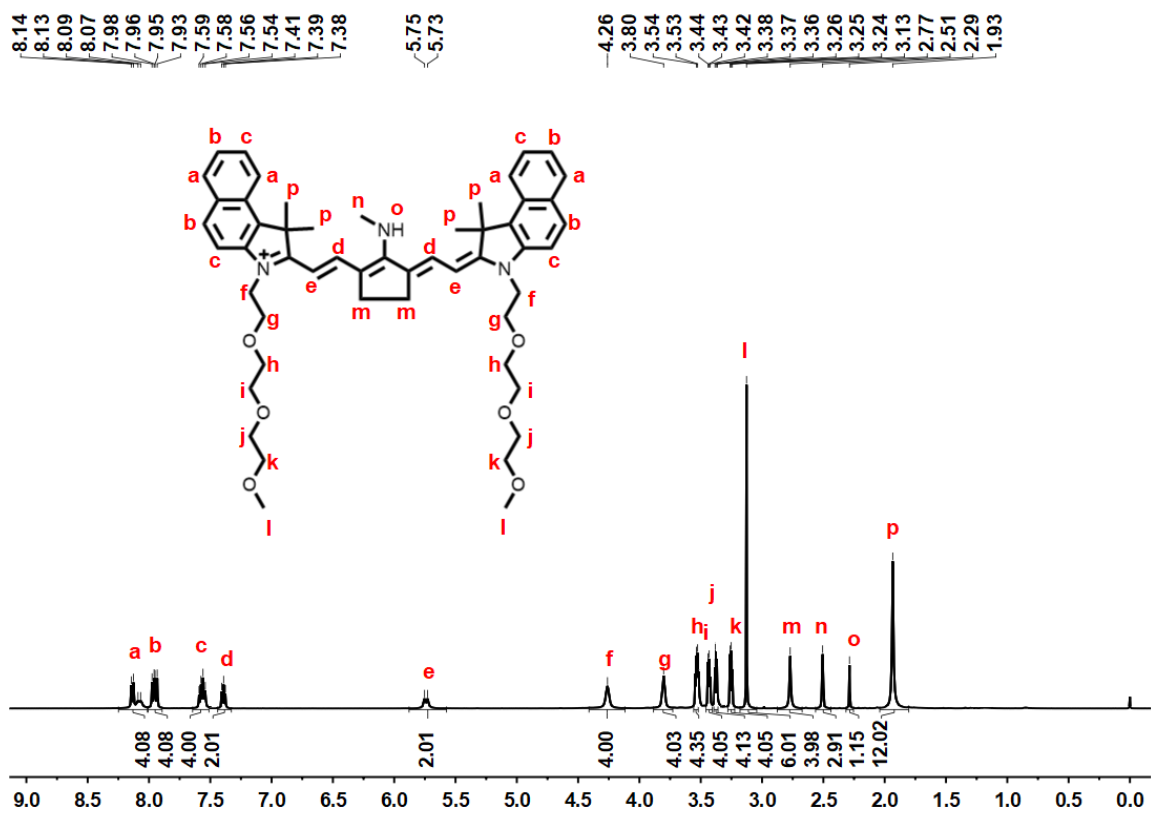


Fig. S3. ¹H NMR spectrum of HC-N in DMSO-d₆.

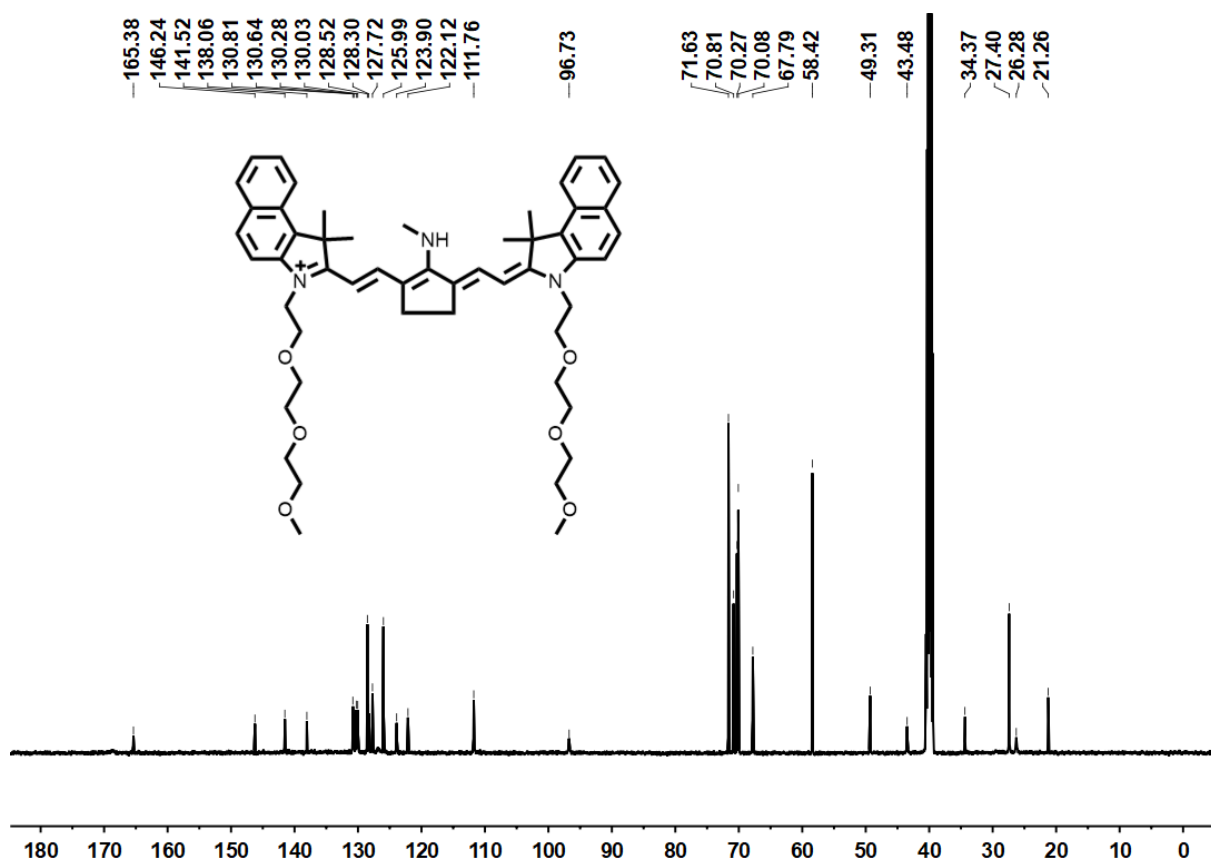


Fig. S4. ^{13}C NMR spectrum of Compound HC-N in DMSO-d_6 .

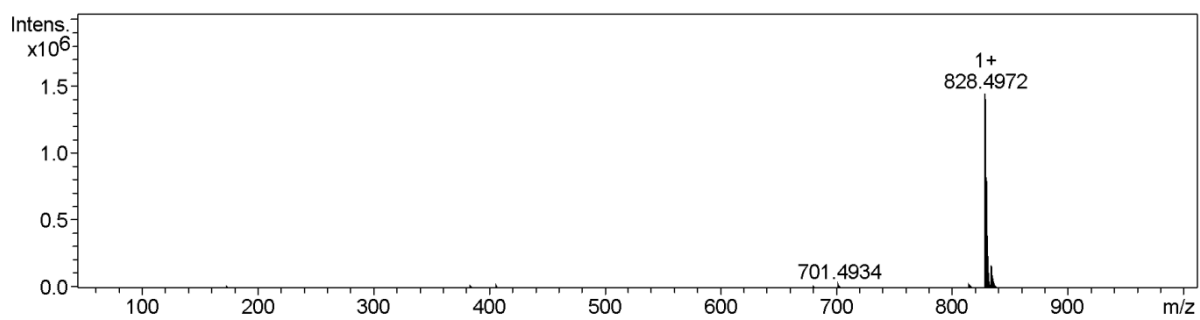


Fig. S5. HR Mass spectrum of Compound HC-N.
 m/z $[\text{M}]^+$ 828.4972

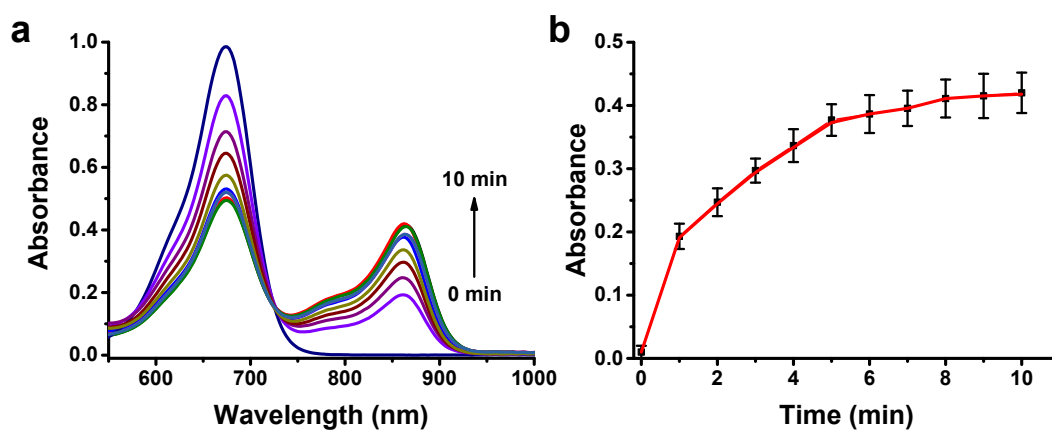


Fig. S6. (a) Time-dependent absorption spectra of the probe HC-N ($5 \mu\text{M}$) in PBS (10 mM , $\text{pH} = 7.4$) upon reaction with MAHMA NONOate ($50 \mu\text{M}$). (b) The plot of absorbance at 865 nm versus time upon reaction with MAHMA NONOate ($50 \mu\text{M}$). ($n = 3$).

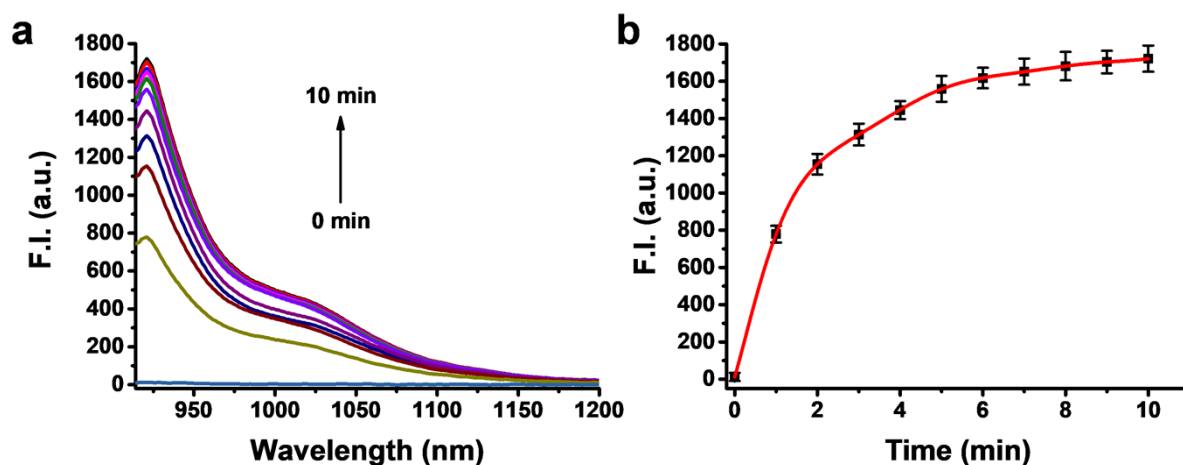


Fig. S7. (a) Time-dependent NIR-II fluorescence spectra of the probe HC-N ($5 \mu\text{M}$) in PBS (10 mM , $\text{pH} 7.4$) upon reaction with MAHMA NONOate ($50 \mu\text{M}$). Excitation laser: 808 nm . (b) The plot of fluorescent intensity at 923 nm versus time upon reaction with MAHMA NONOate ($50 \mu\text{M}$). ($n = 3$).

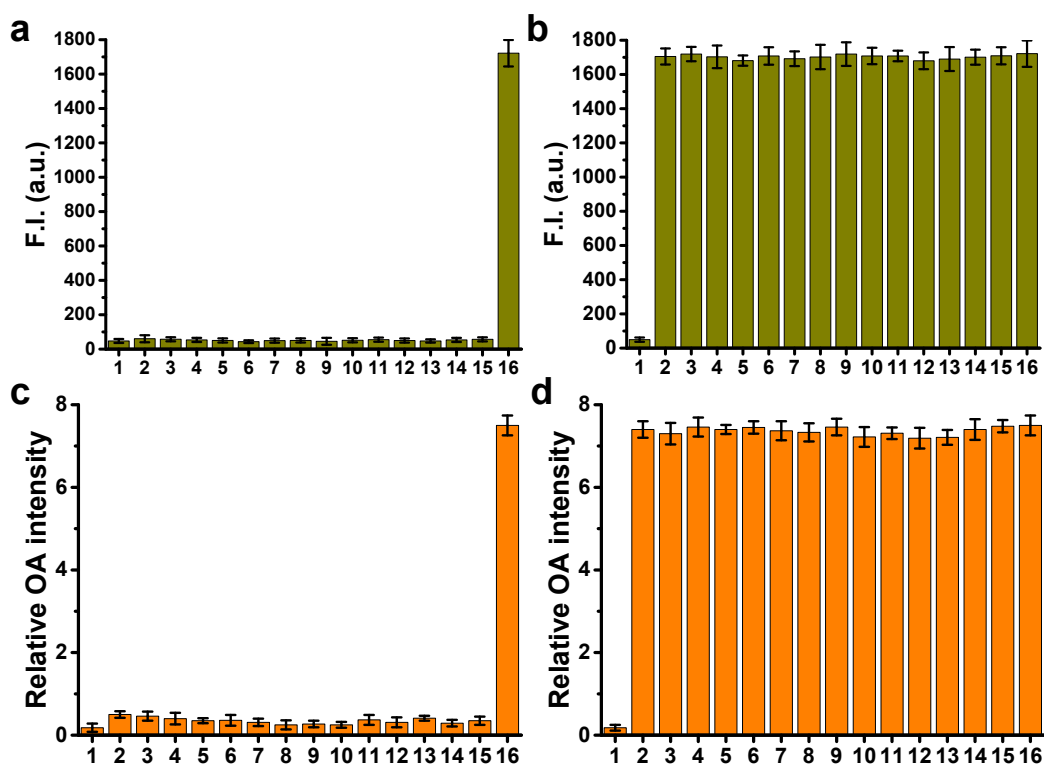


Fig. S8. (a) Fluorescent intensity at 923 nm of the probe HC-N (5 μM) upon incubation with different substances respectively in PBS (10 mM, pH 7.4) at 37 $^{\circ}\text{C}$ for 10 min. (b) Fluorescent intensity at 923 nm of the probe HC-N (5 μM) upon treatment with 50 μM MAHMA NONOate and simultaneously in the presence of individual substance respectively for 10 min in PBS (10 mM, pH 7.4) at 37 $^{\circ}\text{C}$. Excitation laser: 808 nm. (c) Relative optoacoustic intensity of the probe HC-N (5 μM) in the presence of different substances respectively for 10 min in PBS (10 mM, pH 7.4) at 37 $^{\circ}\text{C}$. (d) Relative optoacoustic intensity of the probe HC-N (5 μM) in the presence of 50 μM MAHMA NONOate and simultaneously in the presence of individual substance respectively for 10 min in PBS (10 mM, pH 7.4) at 37 $^{\circ}\text{C}$. (1. Only probe solution with no addition of NO or other substances, 2. 100 μM H_2O_2 , 3. 100 μM ClO^- , 4. 100 μM NO_3^- , 5. 1 mM K^+ , 6. 1 mM Na^+ , 7. 1 mM Ca^+ , 8. 1 mM Cl^- , 9. 1 mM Br^- , 10. 1 mM I^- , 11. 1 mM Glu, 12. 1 mM Tyr, 13. 1 mM Ala, 14. 1 mM Cys, 15. 10 mM GSH, 16. 50 μM MAHMA NONOate). (n = 3).

Fig. S9. (a) HR mass spectrum of the probe HC-N (5 μ M) after being incubated with 50 μ M MAHMA NONOate in PBS (10 mM, pH 7.4) for 1 min at 37 $^{\circ}$ C. (b) Partial enlargement of the spectrum for the peak of HC-NO.

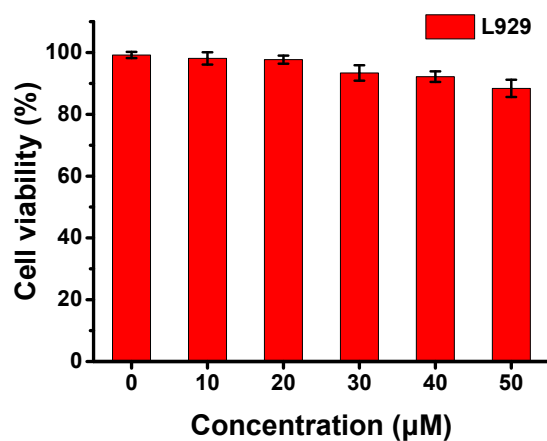


Fig. S10. Cell viabilities of L929 cells incubated with different concentrations (0, 10, 20, 30, 40 and 50 μM) of the probe HC-N by MTT assay. Three independent experiments were performed and eight replicates were performed for each independent experiment. Data represent mean \pm SD. Error bars represent the standard deviation (SD).

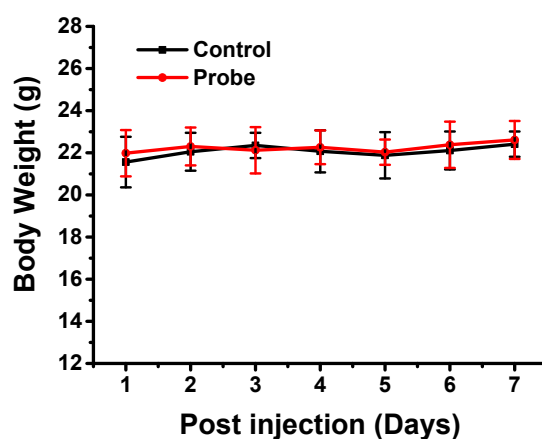


Fig. S11. The body weights' changes of healthy mice within 7d upon intravenously injected with saline (the control) or the probe HC-N ($3.5 \text{ mg}\cdot\text{kg}^{-1}$, in $50 \mu\text{L}$ saline) daily. ($n = 3$).

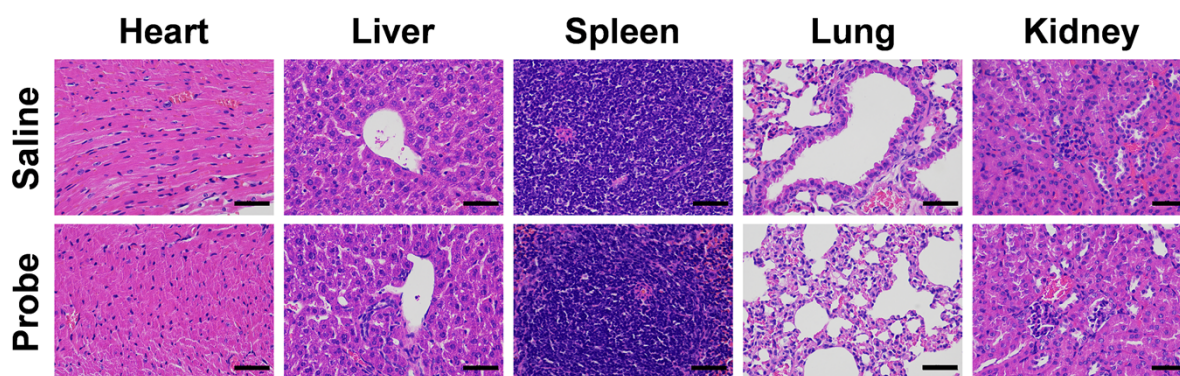


Fig. S12. Representative images of H&E staining for major organs (including hearts, livers, spleens, lungs, and kidneys) excised from the healthy mice at 7d after i.v. injection of saline or the probe HC-N (3.5 mg kg^{-1} , in $50 \mu\text{L}$ saline). Scale bar: $50 \mu\text{m}$.

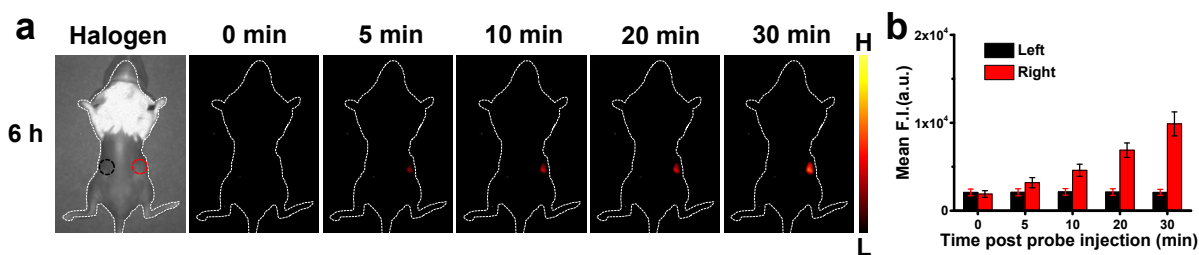


Fig. S13. (a) At 6 hours after LPS-induced acute dermatitis: bright-field image and NIR-II fluorescence images of the mice at different time points (0, 5, 10, 20 and 30 min) after subcutaneous injection of the probe HC-N (3.5 mg kg^{-1} , in $50 \mu\text{L}$ saline). The mice were in prone posture. Red circle: LPS was subcutaneously injected on the right side of the back of mice. Black circle: saline was subcutaneously injected on the left side of the back of mice. Excitation laser: 808 nm. (b) Mean fluorescence intensities at ROI (black and red circle) of the back skin region in mice of (a). ($n = 3$).

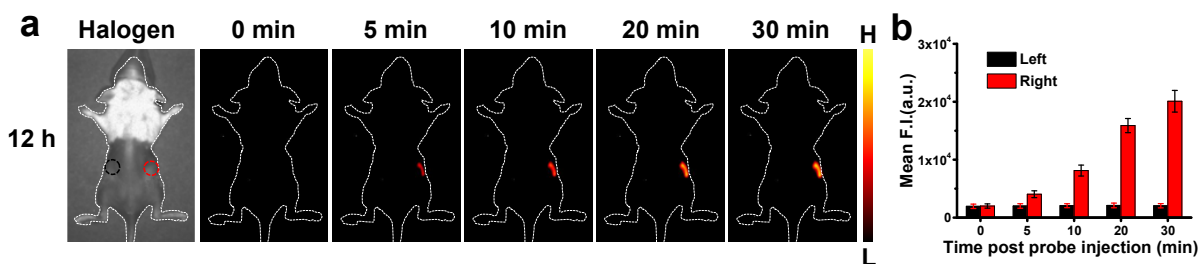


Fig. S14. (a) At 12 hours after LPS-induced acute dermatitis: bright-field image and NIR-II fluorescence images of the mice at different time points (0, 5, 10, 20 and 30 min) after subcutaneous injection of the probe HC-N (3.5 mg kg^{-1} , in $50 \mu\text{L}$ saline). The mice were in prone posture. Red circle: LPS was subcutaneously injected on the right side of the back of mice. Black circle: saline was subcutaneously injected on the left side of the back of mice. Excitation laser: 808 nm. (b) Mean fluorescence intensities at ROI (black and red circle) of the back skin region in mice of (a). ($n = 3$).

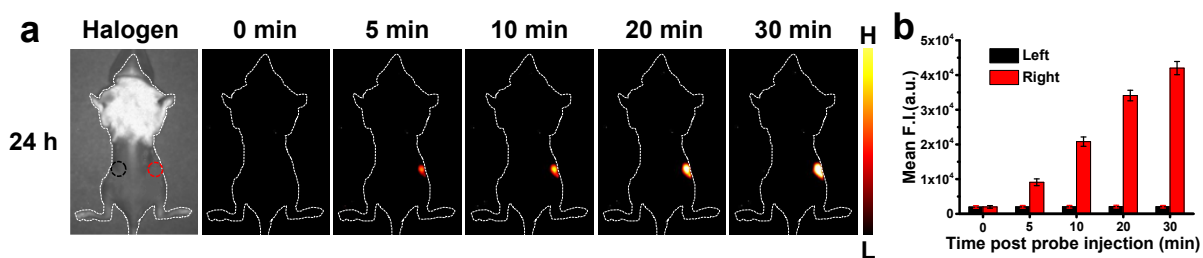


Fig. S15. (a) At 24 hours after LPS-induced acute dermatitis: bright-field image and NIR-II fluorescence images of the mice at different time points (0, 5, 10, 20 and 30 min) after subcutaneous injection of the probe HC-N (3.5 mg kg^{-1} , in $50 \mu\text{L}$ saline). The mice were in prone posture. Red circle: LPS was subcutaneously injected on the right side of the back of mice. Black circle: saline was subcutaneously injected on the left side of the back of mice. Excitation laser: 808 nm. (b) Mean fluorescence intensities at ROI (black and red circle) of the back skin region in mice of (a). ($n = 3$).

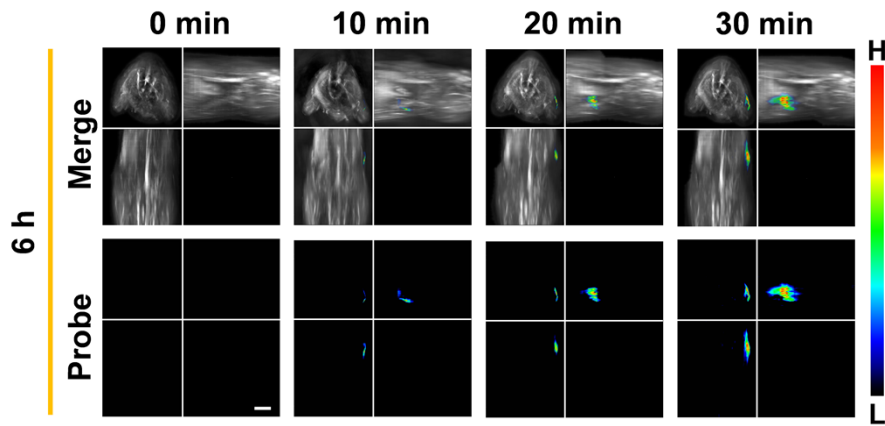


Fig. S16. At 6 hours after LPS-induced acute dermatitis: representative 3D MSOT images of the mice at different time points (0, 10, 20 and 30 min) after subcutaneous injection of the probe HC-N (3.5 mg kg^{-1} , in $50 \mu\text{L}$ saline). The mice were in prone posture. Scale bar: 5 mm.

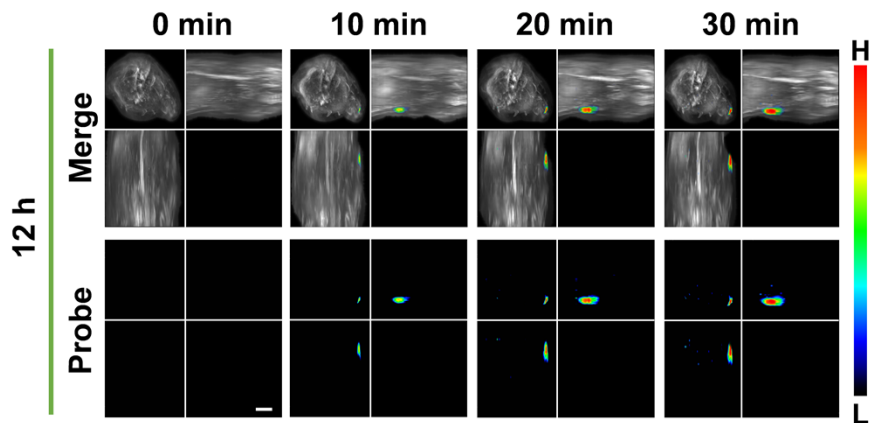


Fig. S17. At 12 hours after LPS-induced acute dermatitis: representative 3D MSOT images of the mice at different time points (0, 10, 20 and 30 min) after subcutaneous injection of the probe HC-N (3.5 mg kg^{-1} , in $50 \mu\text{L}$ saline). The mice were in prone posture. Scale bar: 5 mm.

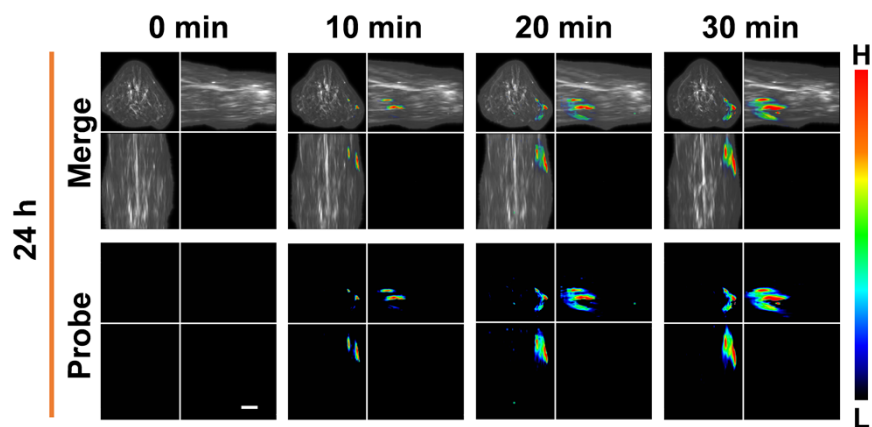


Fig. S18. At 24 hours after LPS-induced acute dermatitis: representative 3D MSOT images of the mice at different time points (0, 10, 20 and 30 min) after subcutaneous injection of the probe HC-N (3.5 mg kg^{-1} , in $50 \text{ }\mu\text{L}$ saline). The mice were in prone posture. Scale bar: 5 mm.

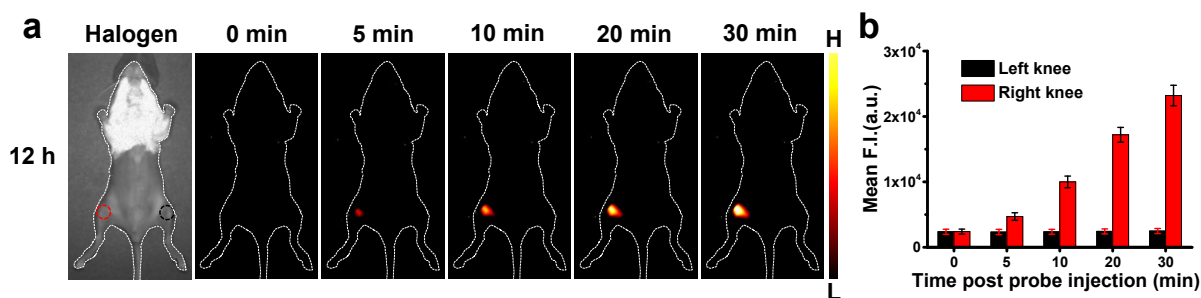


Fig. S19. (a) At 12 hours after MIA-induced acute joint inflammation: bright-field image and NIR-II fluorescence images of the mice at different time points (0, 5, 10, 20 and 30 min) after in situ injection of the probe HC-N (3.5 mg kg^{-1} , in $20 \text{ }\mu\text{L}$ saline). The mice were in supine posture. Red circle: MIA was infrapatellar injected on the right knee joint of mice. Black circle: saline was infrapatellar injected on the left knee joint of mice of mice. Excitation laser: 808 nm. (b) Mean fluorescence intensities at ROI (black and red circle) of the left and right knee joint in mice of (a). ($n = 3$).

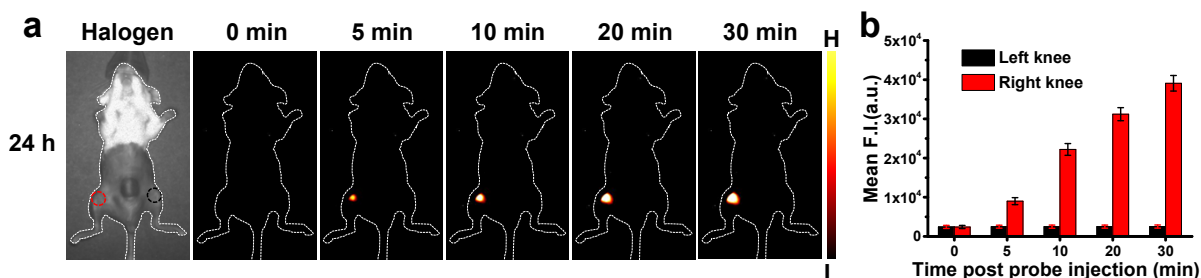


Fig. S20. (a) At 24 hours after MIA-induced acute joint inflammation: bright-field image and NIR-II fluorescence images of the mice at different time points (0, 5, 10, 20 and 30 min) after in situ injection of the probe HC-N (3.5 mg kg^{-1} , in $20 \text{ }\mu\text{L}$ saline). The mice were in supine posture. Red circle: MIA was infrapatellar injected on the right knee joint of mice. Black circle: saline was infrapatellar injected on the left knee joint of mice of mice. Excitation laser: 808 nm. (b) Mean fluorescence intensities at ROI (black and red circle) of the left and right knee joint in mice of (a). ($n = 3$).

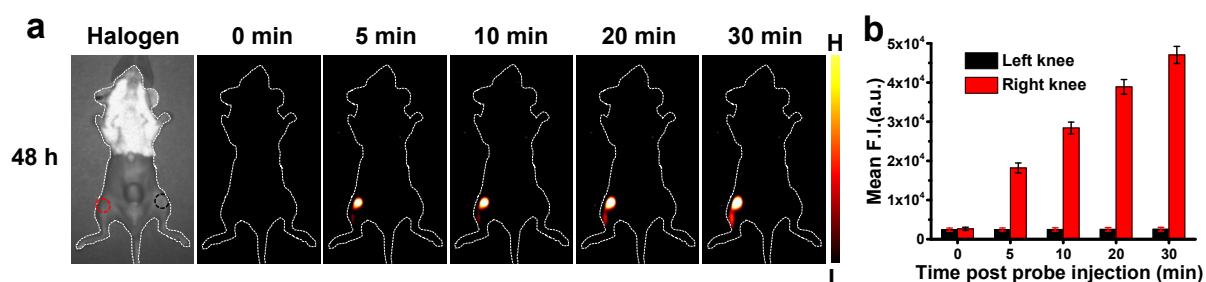


Fig. S21. (a) At 48 hours after MIA-induced acute joint inflammation: bright-field image and NIR-II fluorescence images of the mice at different time points (0, 5, 10, 20 and 30 min) after in situ injection of the probe HC-N (3.5 mg kg^{-1} , in $20 \mu\text{L}$ saline). The mice were in supine posture. Red circle: MIA was infrapatellar injected on the right knee joint of mice. Black circle: saline was infrapatellar injected on the left knee joint of mice of mice. Excitation laser: 808 nm. (b) Mean fluorescence intensities at ROI (black and red circle) of the left and right knee joint in mice of (a). ($n = 3$).

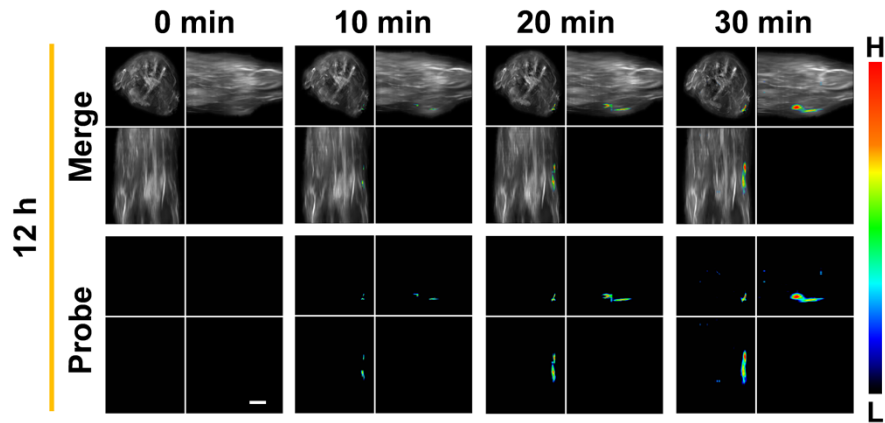


Fig. S22. At 12 hours after MIA-induced acute joint inflammation, representative 3D MSOT images of the mice at different time points (0, 10, 20 and 30 min) after in situ injection of the probe HC-N (3.5 mg kg^{-1} , in $20 \text{ }\mu\text{L}$ saline). The mice were in prone posture. Scale bar: 5 mm. For the 3D MSOT images, the top-left subpanel represents the x-y plane, the top-right subpanel represents the y-z plane, and the bottom-left subpanel represents the x-z plane.

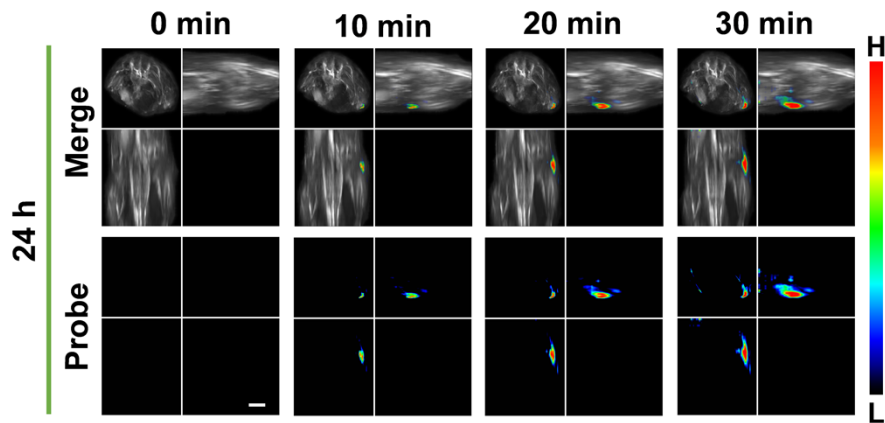


Fig. S23. At 24 hours after MIA-induced acute joint inflammation, representative 3D MSOT images of the mice at different time points (0, 10, 20 and 30 min) after in situ injection of the probe HC-N (3.5 mg kg^{-1} , in $20 \text{ }\mu\text{L}$ saline). The mice were in prone posture. Scale bar: 5 mm. For the 3D MSOT images, the top-left subpanel represents the x-y plane, the top-right subpanel represents the y-z plane, and the bottom-left subpanel represents the x-z plane.

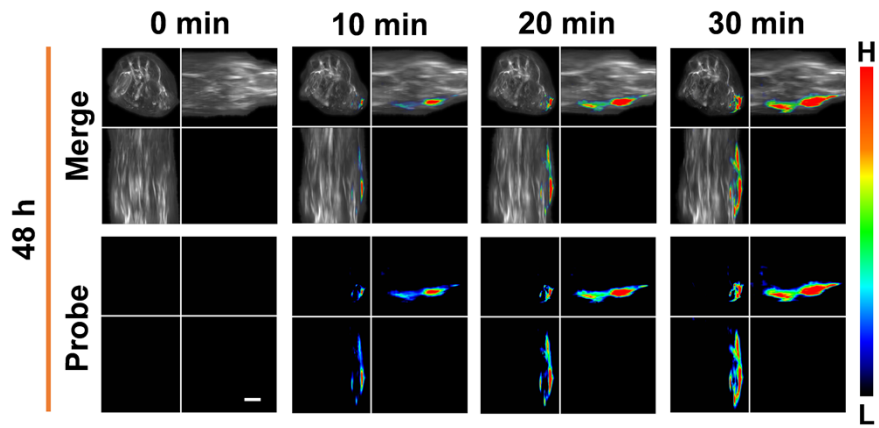
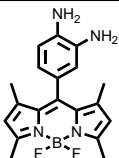
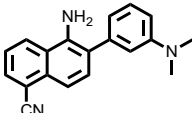
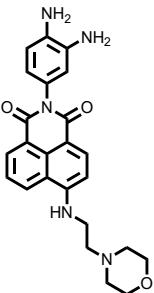
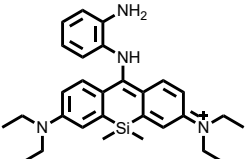
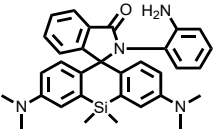
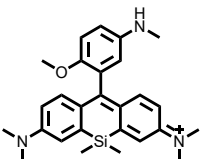
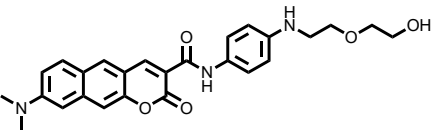
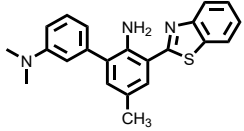
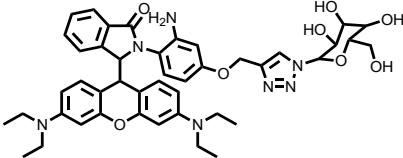
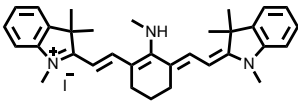
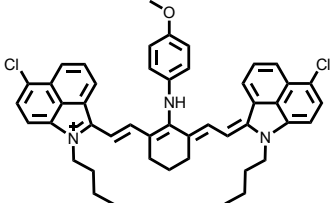
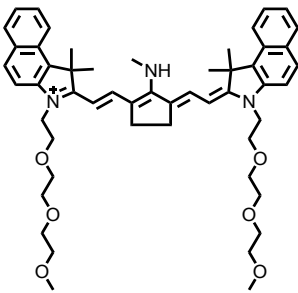


Fig. S24. At 48 hours after MIA-induced osteoarthritis, representative 3D MSOT images of the mice at different time points (0, 10, 20 and 30 min) after in situ injection of the probe HC-N (3.5 mg kg^{-1} , in $20 \text{ }\mu\text{L}$ saline). The mice were in prone posture. Scale bar: 5 mm. For the 3D MSOT images, the top-left subpanel represents the x-y plane, the top-right subpanel represents the y-z plane, and the bottom-left subpanel represents the x-z plane.

Table S1. Comparison of the probe in this work and the literature-reported probes for NO detection and related applications

Probe structure	Fluorescence imaging	Optoacoustic imaging	Applications	Ref.
	Visible light range	/	NO detection in buffer solution.	3
	Visible light range	/	Fluorescent imaging of NO in living cells.	4
	Visible light range	/	Fluorescent imaging of endogenous NO in lysosomes of macrophage cells.	5
	NIR-I	/	Detecting NO activity in Hela cell.	6
	NIR-I	/	Fluorescent imaging of endogenous NO in living cells and in abdominal cavity of mouse.	7
	NIR-I	/	Fluorescent imaging NO in a mouse model of xenograft tumor.	8
	NIR-I	/	Fluorescent imaging of NO in a mouse kidney ischemia-reperfusion injury model.	9

	NIR-I	/	Monitoring NO in HeLa cells.	10
	NIR-I	/	Real-time imaging of hepatocellular NO in both HepG2 cells and zebrafish.	11
	NIR-I	/	Fluorescent imaging of exogenous and endogenous NO in mouse's skin.	12
	NIR-II	Optoacoustic imaging	NIR-II fluorescent and photoacoustic imaging of endogenous NO in breast and liver cancer mouse models.	13
	NIR-II	Optoacoustic imaging (3D-MSOT imaging)	NIR-II fluorescence and 3D-MSOT dual mode imaging for detecting LPS-induced dermatitis and MIA-induced osteoarthritis in mice via in-situ detection of NO.	This work

Reference

- [1] C. Zeng, J. Ouyang, L. Sun, Z. Zeng, Y. Tan, F. Zeng and S. Wu, *Anal. Chim. Acta.*, 2022, **1208**, 339831.
- [2] Y. Huang, Y. Qi, C. Zhan, F. Zeng and S. Wu, *Anal. Chem.*, 2019, **91**, 8085-8092.
- [3] Y. Gabe, Y. Urano, K. Kikuchi, H. Kojima and T. Nagano, *J. Am. Chem. Soc.*, 2004, **126**, 3357-3367.
- [4] Y. Yang, S. K. Seidlits, M. M. Adams, V. M. Lynch, C. E. Schmidt, E. V. Anslyn and J. B. Shear, *J. Am. Chem. Soc.*, 2010, **132**, 13114-13116.
- [5] H. Yu, Y. Xiao and L. Jin, *J. Am. Chem. Soc.*, 2012, **134**, 17486-17489.
- [6] J. Tang, Z. Guo, Y. Zhang, B. Bai and W. Zhu, *Chem. Commun.*, 2017, **53**, 10520-10523.
- [7] Y. Huo, J. Miao, L. Han, Y. Li, Z. Li, Y. Shi and W. Guo, *Chem. Sci.*, 2017, **8**, 6857-6864.
- [8] Z. Mao, H. Jiang, X. Song, W. Hu and Z. Liu, *Anal. Chem.*, 2017, **89**, 9620-9624.
- [9] Z. Mao, H. Jiang, Z. Li, C. Zhong, W. Zhang and Z. Liu, *Chem. Sci.*, 2017, **8**, 4533-4538.
- [10] L. Chen, D. Wu and J. Yoon, *Sens. Actuators B Chem.*, 2018, **259**, 347-353.
- [11] P. Zhang, Y. Tian, H. Liu, J. Ren, H. Wang, R. Zeng, Y. Long and J. Chen, *Chem. Commun.*, 2018, **54**, 7231-7234.
- [12] Y. Liu, H. Fan, Y. Wen, T. Jia, Q. Su and F. Li, *Dyes Pigments.*, 2019, **166**, 211-216.
- [13] M. Y. Lucero, A. K. East, C. J. Reinhardt, A. C. Sedgwick, S. Su, M. C. Lee and J. Chan, *J. Am. Chem. Soc.*, 2021, **143**, 7196-7202.